

Diffusion-weighted MRI of urinary bladder and prostate cancers

Özgür Kılıçkesmez, Tan Cimilli, Ercan İnci, Arda Kayhan, Sibel Bayramoğlu, Neslihan Taşdelen, Nevzat Gürmen

PURPOSE

The purpose of this study was to evaluate the feasibility of diffusion-weighted imaging in the diagnosis of the urinary bladder and prostate carcinomas. The apparent diffusion coefficient (ADC) values of the malignant and normal tissues were correlated.

MATERIALS AND METHODS

A total of 23 patients with 14 urinary bladder carcinomas and 9 prostate carcinomas, and 50 healthy controls with normal ultrasonographic urinary bladder and prostate gland imaging findings were enrolled in the study. The ADC values were reported as the mean \pm standard deviation. Student's *t* test was performed to compare the ADC values of the normal and pathological tissues. Diffusion-weighted imaging (DWI) was performed with *b* factors of 0, 500, and 1000 s/mm², and the ADC values of the normal tissues and lesions were calculated.

RESULTS

The mean ADC value of the urinary bladder wall of the control group and bladder carcinomas were ($2.08 \pm 0.22 \times 10^{-3}$ mm²/s) and ($0.94 \pm 0.18 \times 10^{-3}$ mm²/s), respectively. In addition, the ADC values of the normal peripheral ($2.07 \pm 0.33 \times 10^{-3}$ mm²/s), transitional zones ($1.46 \pm 0.23 \times 10^{-3}$ mm²/s) of the prostate, seminal vesicles ($2.13 \pm 0.13 \times 10^{-3}$ mm²/s) and the prostate carcinomas ($1.06 \pm 0.17 \times 10^{-3}$ mm²/s) were calculated. The comparison of mean ADC values of the peripheral-transitional zones of the prostate, normal bladder wall-bladder carcinomas, and peripheral zone prostate carcinomas were statistically significant ($P < 0.01$).

CONCLUSION

The present study demonstrated that ADC measurement has a potential ability to differentiate carcinomas from normal bladder wall and prostate gland.

Key words: • diffusion magnetic resonance imaging
• urinary bladder • prostate

Prostate cancer is the third leading cause of death and is the most common genitourinary malignancy in men. Cancer of the urinary bladder is the second most common malignancy of the genitourinary system (1, 2). For the radiological evaluation of the urinary bladder and prostate gland, magnetic resonance imaging (MRI) is a valuable imaging modality due to high tissue contrast, multiplanar imaging capabilities, and the possibility of tissue characterization (3). In addition, many new techniques in bladder imaging, and especially prostate gland MRI, are under development and refinement (1, 4).

Recently, diffusion-weighted imaging (DWI) has emerged as a diagnostic technique in the evaluation of various abdominal lesions. DWI reveals micro-molecular diffusion, which is the Brownian motion of the spins in biologic tissues. This technique can delineate pathologic lesions with high tissue contrast against generally suppressed background signal. The apparent diffusion coefficient (ADC) value has been reported to be useful for quantitatively distinguishing malignancy from benign lesions (5, 6). We sought to present DWI features of bladder and prostate carcinomas, and to evaluate its ability to detect malignancy.

Materials and methods

Patients

During a period of six months, a total of 23 patients with 14 urinary bladder transitional cell carcinomas (mean age, 52 years), and nine prostatic adenocarcinomas (mean age, 61 years), and 50 healthy controls (mean age, 43 years) with normal ultrasonographic and magnetic resonance urinary bladder and prostate gland imaging findings were enrolled in the study. The control group consisted of 30 volunteers and 20 patients who underwent abdominal MRI for reasons unrelated to the urogenital system. Because the control group consisted of men, three women with bladder carcinomas were excluded from the imaging study. The research protocol was approved by the ethics committee. Written consent was obtained from all patients prior to commencement of the study. The final diagnoses of the patients were made by histopathological examination. All patients with prostatic carcinoma received an extended 8- to 16-core transrectal ultrasound (TRUS)-guided biopsy, an improvement of the sextant TRUS-guided biopsy procedure. Biopsy sites common to all patients were the bilateral peripheral zones including the base, mid gland, and apex, and the bilateral transitional zones. Additional sites were included if cancerous lesions were strongly suspected on the basis of T2-weighted and DW images.

MR imaging

MRI was performed on a 1.5 T body scanner (Avanto; Siemens, Erlangen, Germany) with a 33 mT/m maximum gradient capability using an

From the Department of Radiology (Ö.K. ✉ okilickesmez@yahoo.com, N.T., N.G.), University of Yeditepe School of Medicine, İstanbul, Turkey; the Department of Radiology (T.C., E.I., S.B.), Bakırköy Dr. Sadi Konuk Training and Research Hospital, İstanbul, Turkey; and the Department of Radiology (A.K.), Namik Kemal University School of Medicine, Tekirdağ, Turkey.

Received 10 September 2008; revision requested 21 October 2008; revision received 25 November 2008; accepted 25 November 2008.

eight channel phased-array body coil. Before DWI, breathhold axial fat saturated 3D gradient-echo T1-weighted (repetition time [TR], 5.32 ms; echo time [TE], 2.53 ms; flip angle [FA], 10°), axial turbo spin-echo T2-weighted sequence (TR, 5030 ms; TE, 101 ms; FA, 150°), sagittal turbo spin-echo T2-weighted sequence (TR, 4320 ms; TE, 87 ms; FA, 150°), axial turbo spin-echo T1-weighted sequence (TR, 536 ms; TE, 11 ms; FA, 150°), coronal turbo spin-echo TIRM sequence (TR, 4980 ms; TE, 84 ms; FA, 150°) and then diffusion weighted single-shot spin-echo echo-planar sequence with chemical shift selective fat-suppression technique (TR/TE, 4900/93); matrix, 192 × 192; slice numbers, 30; slice thickness, 6 mm; interslice gap, 35%; FOV, 45 cm; averages, 5; acquisition time, approximately 3 minutes; PAT factor, 2; PAT mode, parallel imaging with modified sensitivity encoding (mSENSE) were performed. DWI was performed with b factors of 0, 500, and 1000 s/mm².

Following DWI, contrast enhanced imaging was performed with axial, coronal, and sagittal fat-saturated 3D gradient-echo T1-weighted MR sequence after administration of gadopentetate dimeglumine, with a dose of 0.1 mmol/kg of body weight as a bolus injection.

Image interpretation

DWI datasets were transferred to an independent workstation (Leonardo console, software version 2.0; Siemens) for postprocessing, and the ADC maps were reconstructed. To measure the ADC value of bladder wall, seminal vesicles, and prostate gland peripheral and transitional zones, we established round regions of interest (ROIs). The ROIs were selected by consensus of two radiologists. In the patient group, a free-hand ROI was defined for the lesions detected on the T2-weighted EPI image (b = 0), while referring to the conventional sequences for verification of the lesion boundaries. The ROI was then copied to the corresponding ADC map.

Statistical analysis

All statistical analyses were performed using Statistical Package for Social Sciences for Windows 10.0 (SPSS Inc., Chicago, USA). The ADC values of cases were reported as the mean ± standard deviation. Student's t test was

performed to compare the ADC values of the normal and pathological tissues. A value of $P < 0.05$ was considered to indicate a statistically significant difference.

Results

The ADC values of the normal prostate zones, bladder wall, and carcinomas are listed in Table. The mean ADC values of the peripheral and transitional zones of the prostate gland yielded a statistically significant difference. Also the ADC values of normal bladder wall, bladder carcinomas, and the prostate peripheral zone-prostate carcinomas were significantly different ($P < 0.01$). The correlation of the normal prostate gland, transitional zone carcinoma, and prostate carcinomas yielded a statistically significant difference ($P < 0.05$). Representative cases and the scatter plots are shown in Figs. 1–5.

Discussion

DWI is a recently introduced technique that depicts differences in molecular diffusion caused by the random and microscopic motion of molecules, which is known as Brownian motion (5, 7). Restriction to the molecular diffusion of water in neoplastic tissues can be related both to the greater cellular density in the tissues, generated by the high index of neoplastic replication with a consequent reduction in the width of intercellular spaces, and to the ultrastructural alteration of the normal tissues.

In prostate cancer, normal glandular architecture is disrupted, and is replaced by aggregated cancer cells and fibrotic stroma. These changes inhibit the movement of water molecules,

with resultant restriction of diffusion and reduction of ADC values in the cancer tissue (8).

There are many studies of normal and cancerous tissue discrimination of the prostate gland; however, there are only a few studies concerning the DWI of urinary bladder (9–15). The reported ADC values of the normal peripheral (1.60–1.97 × 10⁻³ mm²/s), transitional zones (1.27–1.79 × 10⁻³ mm²/s), and cancers (0.90–1.38 × 10⁻³ mm²/s) of the prostate gland vary in the literature. The differences may be related to the strength of the diffusion gradient (300–1,000 s/mm²), and the magnetic field (1.5 or 3 T) used (10–12, 16). It has been shown that the b value negatively influences the signal-to-noise ratio (SNR) of the image, even though it does not render the sequence less sensitive to the motion of capillary flow and breathing (17). We have found ADC values of the normal zones and cancers similar to those reported in the literature. The study by Tamada et al. (18) described an increase in ADC values of the prostate gland with age. They have also found uniform distribution of the ADC values between different regions of the peripheral or transitional zones of the prostate gland. The mean ADC values of the tumors were significantly lower than ADC values of the normal parenchyma; however, the receiver operated characteristic (ROC) analysis did not demonstrate a reliable cut-off value for the detection of tumors. In our study, six of the nine peripheral zone masses were readily detected with hyperintensity on the DWI; however, all of these masses were hypointense on ADC maps. In contrast, all of the urinary bladder cancers were hyperin-

Table. Normal and pathological apparent diffusion coefficient (ADC) values of the urinary bladder and prostate glands

	n	Mean ADC (mm ² /s)
Normal PZ of prostate	50	2.07 ± 0.33 × 10 ⁻³
Normal TZ of prostate	50	1.46 ± 0.23 × 10 ⁻³
Normal bladder wall	50	2.08 ± 0.22 × 10 ⁻³
Seminal vesicles	50	2.13 ± 0.13 × 10 ⁻³
Bladder carcinomas	13	0.94 ± 0.18 × 10 ⁻³
Prostate carcinomas	9	1.06 ± 0.17 × 10 ⁻³

PZ, peripheral zone; TZ, transitional zone

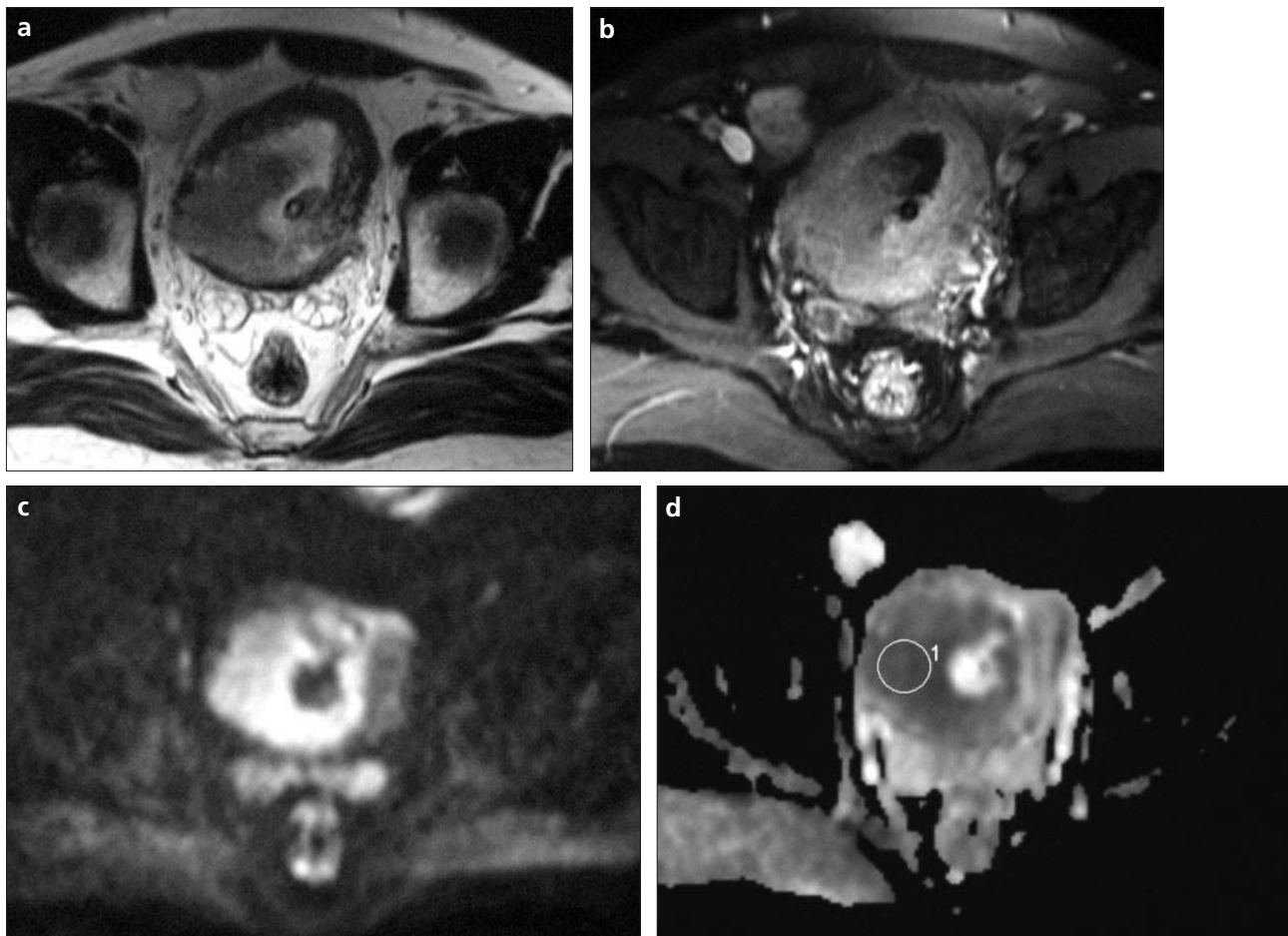


Figure 1. a–d. MR images of urinary bladder carcinoma in a 66-year-old man. Axial TSE T2-weighted image (a) shows a large mass almost completely filling the bladder lumen. Axial post contrast fat saturated VIBE image (b) reveals the enhancement of the large mass. Axial diffusion-weighted ($b = 1,000 \text{ s/mm}^2$) image (c) clearly depicts the tumor with marked hyperintensity. Tumor on ADC image (d) shows hypointensity (restricted diffusion) compared with normal wall. Region of interest (ROI) was placed on the tumor (d). ADC of tumor was $1.13 \times 10^{-3} \text{ mm}^2/\text{s}$.

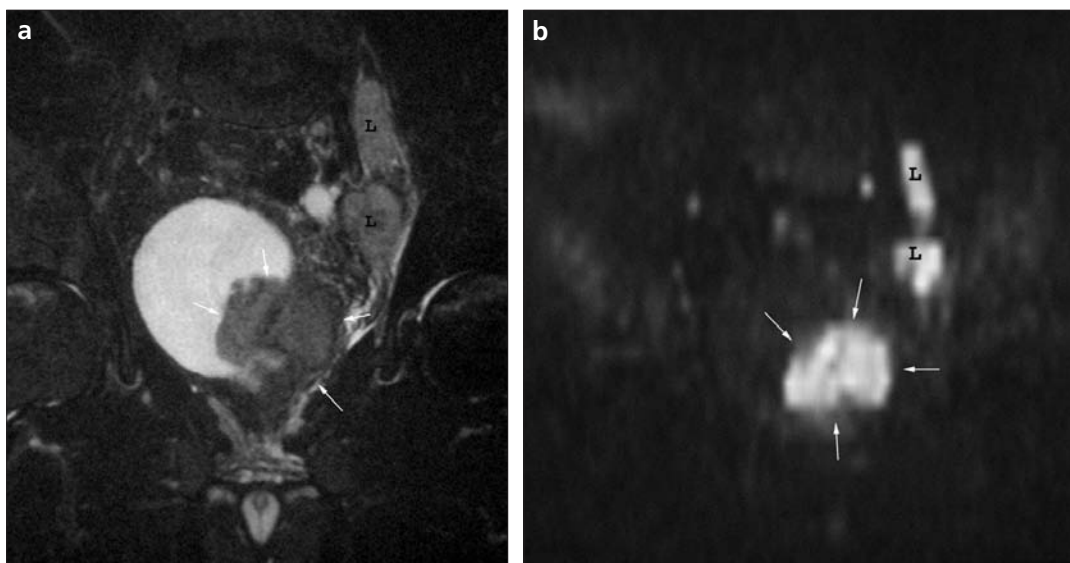


Figure 2. a, b. MR images of urinary bladder carcinoma in a 54-year-old man. Coronal fat saturated T2-weighted image (a) shows a large mass (arrows) protruding into the bladder lumen, arising adjacent to the left ureterovesical junction. Along the internal iliac ring, conglomerated metastatic lymph nodes (L) are seen (a). Diffusion-weighted ($b = 1,000 \text{ s/mm}^2$) image (b) clearly depicts the tumor, and lymph nodes (L) probably with metastatic tumor, with marked hyperintensity. The apparent diffusion coefficient values of the tumor and lymph nodes were calculated as $1.06 \times 10^{-3} \text{ mm}^2/\text{s}$, and $1.22 \times 10^{-3} \text{ mm}^2/\text{s}$ respectively (not shown).

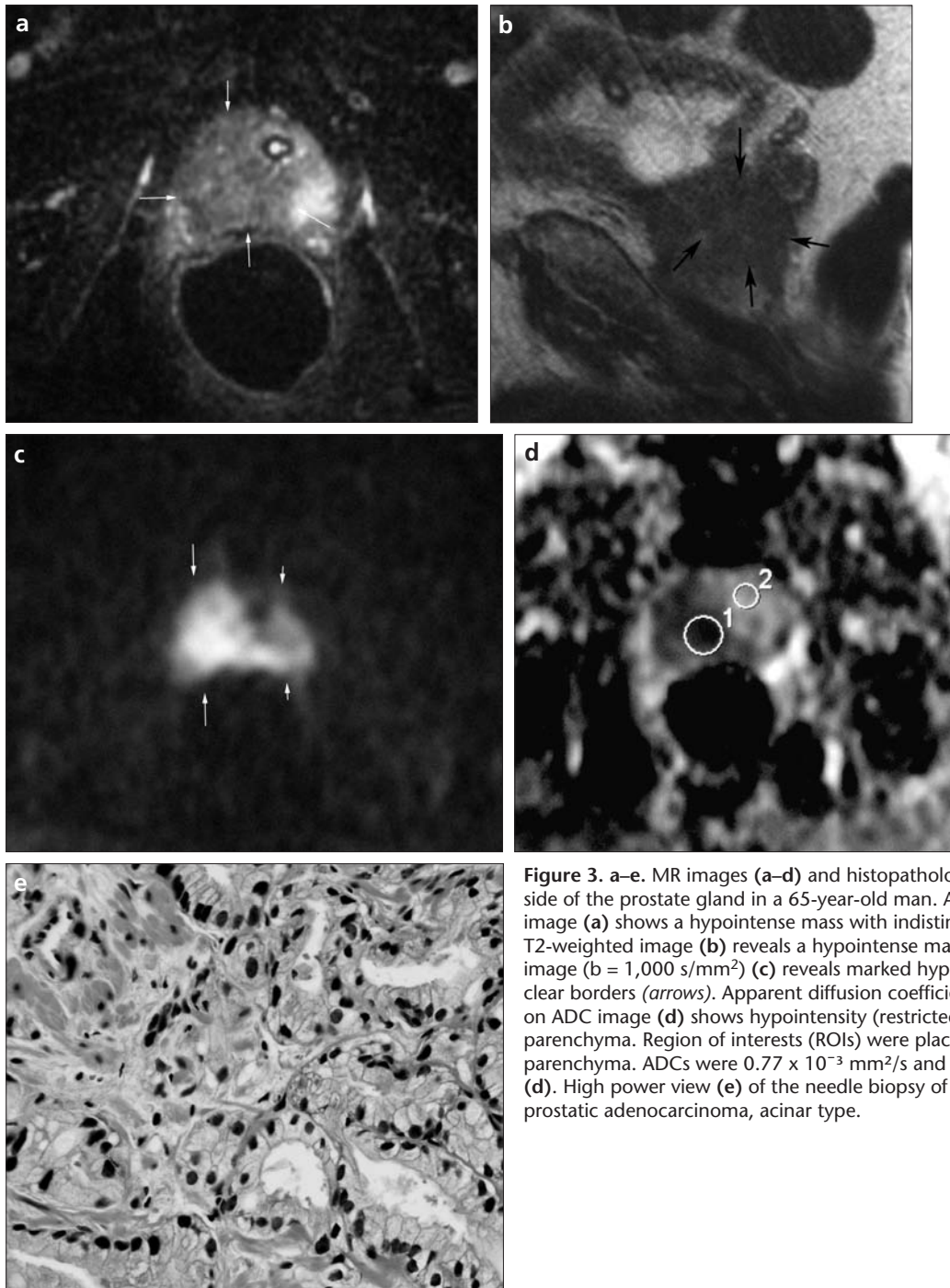


Figure 3. a–e. MR images (a–d) and histopathologic view (e) of cancer on the right side of the prostate gland in a 65-year-old man. Axial fat saturated T2-weighted image (a) shows a hypointense mass with indistinct borders (arrows). Sagittal TSE T2-weighted image (b) reveals a hypointense mass (arrows). Diffusion-weighted image ($b = 1,000 \text{ s/mm}^2$) (c) reveals marked hyperintensity of the mass with more clear borders (arrows). Apparent diffusion coefficient (ADC) was calculated. Tumor on ADC image (d) shows hypointensity (restricted diffusion) compared with normal parenchyma. Region of interests (ROIs) were placed on the mass and normal parenchyma. ADCs were $0.77 \times 10^{-3} \text{ mm}^2/\text{s}$ and $1.40 \times 10^{-3} \text{ mm}^2/\text{s}$, respectively (d). High power view (e) of the needle biopsy of the prostate specimen reveals prostatic adenocarcinoma, acinar type.

tense on DWI. Haider et al. (13) have reported that T2-weighted imaging combined with DWI is better than T2-weighted imaging alone.

Moreover, Miao et al. (19) have found the performance of DWI better than that of T2-weighted imaging in detecting prostate cancer. Researchers who have studied the prostate gland DWI at 3T MRI have reported good performance of high magnetic field as a result of high spatial resolution (11, 19).

A study by Ren et al. (16) reported that DWI was able to discriminate normal prostate gland, benign prostatic hyperplasia (BPH) nodules, cysts, and carcinomas. In this study, the ADC values of BPH nodules were between those of normal parenchyma and those of cancers.

In the literature, there are a few reports evaluating the feasibility of DWI in the diagnosis of urinary bladder cancers. Matsuki et al. (14) have reported

the ADC value of bladder cancers to be lower than that of normal bladder wall, prostate, and seminal vesicles. In concordance with the results of their study, all the bladder cancers we have evaluated were clearly detectable with DWI. These investigators have stated that there was no overlap between the ADC values of tumors and those of normal bladder wall; however, they did not define a cut-off value. In contrast to their study, despite the significant difference

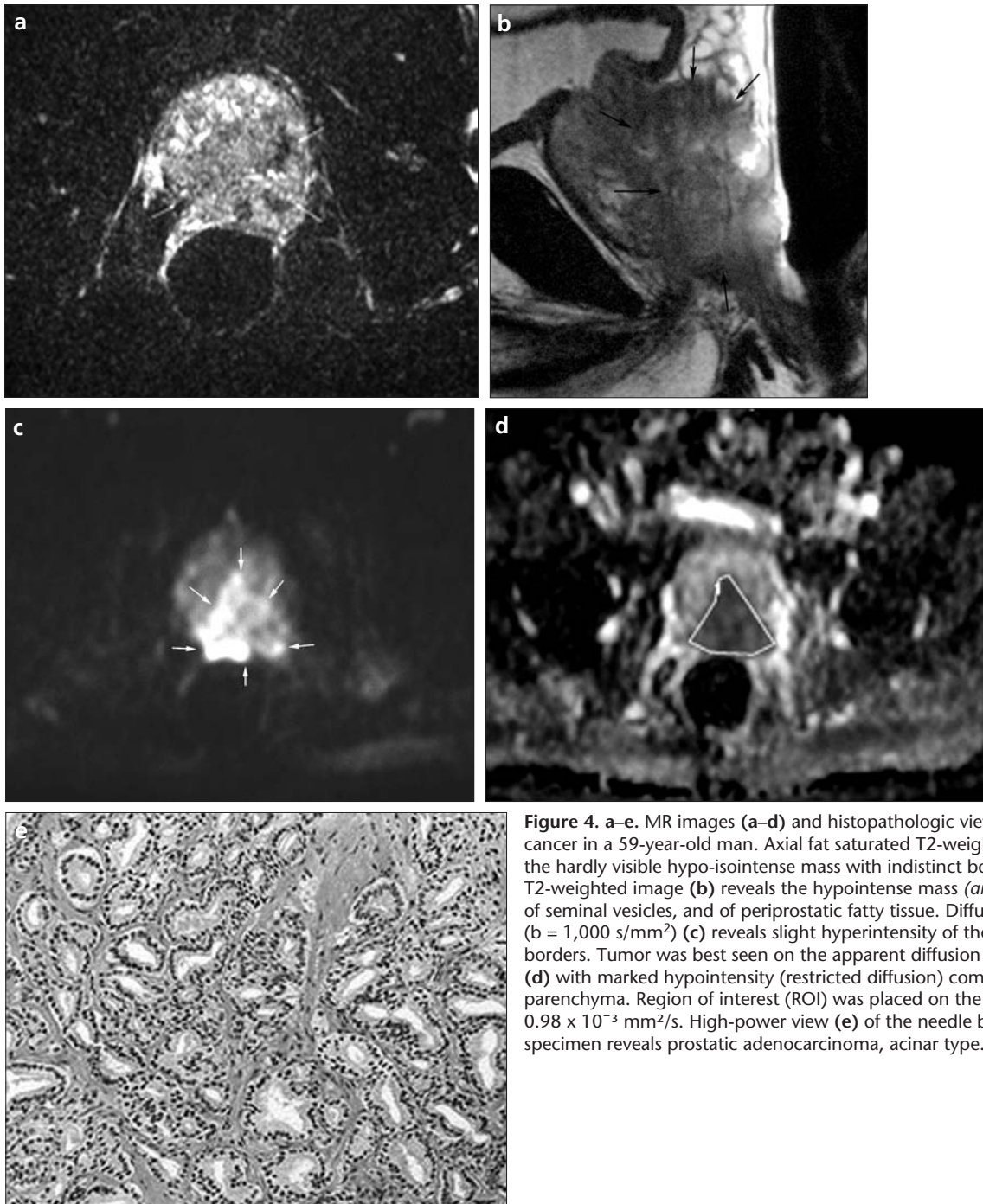


Figure 4. a–e. MR images (a–d) and histopathologic view (e) of prostate cancer in a 59-year-old man. Axial fat saturated T2-weighted image (a) shows the hardly visible hypo-isointense mass with indistinct borders. Sagittal TSE T2-weighted image (b) reveals the hypointense mass (arrows), with invasion of seminal vesicles, and of periprostatic fatty tissue. Diffusion-weighted image ($b = 1,000 \text{ s/mm}^2$) (c) reveals slight hyperintensity of the mass with more clear borders. Tumor was best seen on the apparent diffusion coefficient (ADC) image (d) with marked hypointensity (restricted diffusion) compared with normal parenchyma. Region of interest (ROI) was placed on the mass (d). ADC was $0.98 \times 10^{-3} \text{ mm}^2/\text{s}$. High-power view (e) of the needle biopsy of the prostate specimen reveals prostatic adenocarcinoma, acinar type.

of the ADC values of tumors and bladder wall in our study, there was a small amount of overlap, and we could not determine a cut-off point for the detection of malignancy. In another study, El-Assmy et al. (15) found both sensitivity and specificity of 100% for DWI in the detection of superficial bladder tumors. Similar to our results, they have described an overlap between tumors and the bladder wall; they did not describe a clear cut-off value either.

DWI has advantages such as short acquisition time and high contrast resolution between tumors and normal tissue. However, this technique is limited by poor spatial resolution and the potential risk of image distortion caused by post-biopsy hemorrhage, which results in magnetic field inhomogeneity (8).

White et al. (20) detected post biopsy hemorrhage in 81% of the patients who underwent prostate gland imag-

ing in less than 21 days after biopsy, and, in a second group, hemorrhage was detected in 49% of the patients who underwent imaging 21 days after the procedure. They have also observed a small group demonstrating hemorrhagic changes persisting as long as 4½ months. Staging the cancerous lesions was improved from 46% to 83% after the first 21 days. Because the hemorrhagic foci are seen as hyperintense foci on DWI with lower ADC values,

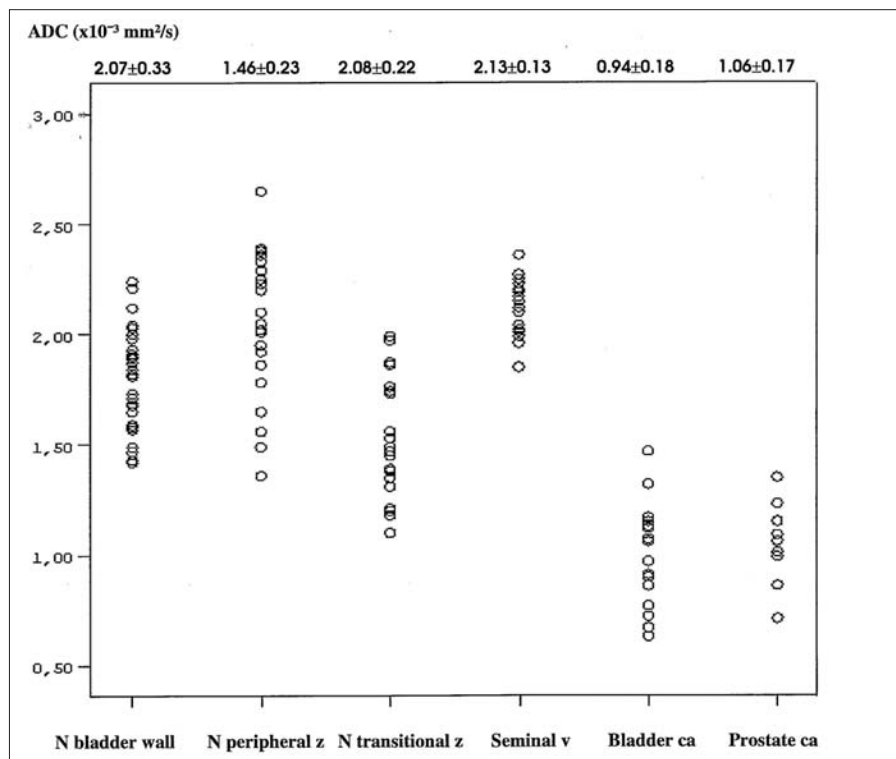


Figure 5. Scatter plots of apparent diffusion coefficient (ADC) values of the normal parenchyma and abnormal tissue (ca, carcinoma; N, normal; v, vesicule; z, zone)

care must be taken to avoid misinterpretation of hemorrhages as cancers. In a recent study by Tamada et al. (21), the sensitivity, specificity, and accuracy of combined T2-weighted, dynamic contrast-enhanced, and DWI in the diagnosis of prostate cancer were 69%, 85%, and 78%, respectively. Sensitivity and specificity were lower for the transitional zone than for the peripheral zone. Degree of hemorrhage was significantly lower in regions of positive biopsy findings than in regions of negative biopsy findings ($P = 0.001$) and correlated negatively with tumor size ($P = 0.043$).

The advantage of the technique was clear depiction of tumors against suppressed background signal. All of the malignant lesions were seen easily with high signal on DWI. Also in our study, DWI was performed without breath holding, thus allowing examination of severely ill, old, or obese patients who were unable to hold their breath for a long time. Although there were ghost and motion artifacts degrading the image quality, they were not severe enough to affect the diagnosis.

DWI may be added to routine abdominal imaging protocols, and visual assessment of DW images may add

confidence to lesion detection and characterization against suppressed background signal, especially in urinary bladder cancers. The use of ADC maps may increase the conspicuity of prostate cancers. The additional benefit of DWI is the ability to determine quantitative indices, which may be important in the assessment of disease response to treatment methods. Conventional assessment by measuring lesion size is insensitive to early treatment-related changes (22).

The present study has several potential limitations. First, the patient population was relatively small. Second, not all of the lesions which may demonstrate similar ADC values were studied. DWI should be assessed with larger groups, in studies including other types of focal lesions. Third, even though the appearance of the prostate gland in the control group was normal, a focus of cancer in the ROIs could not be ruled out. Comparison of DWI images with total histological specimens following radical prostatectomy is required before more meaningful conclusions can be drawn. Our results should be confirmed by additional studies, with radical prostatectomy and whole-mount step-section examination.

In conclusion, DWI provides excellent images of malignant lesions of the bladder and prostate, against suppressed background signal. The use of this technique in conjunction with conventional sequences, may overcome the problem of overlapping values. DWI may be added to routine sequences.

References

- Cornfeld DM, Weinreb JC. MR imaging of the prostate: 1.5T versus 3T. *Magn Reson Imaging Clin N Am* 2007; 15:433-448.
- Zhang J, Gerst S, Lefkowitz RA, Bach A. Imaging of bladder cancer. *Radiol Clin North Am* 2007; 45:183-205.
- Renken NS, Krestin GP. Magnetic resonance imaging of the kidney. *Semin Ultrasound CT MR* 2005; 26:153-161.
- Fütterer JJ, Heijmink SW, Spermon JR. Imaging the male reproductive tract: current trends and future directions. *Radiol Clin North Am* 2008; 46:133-147.
- Le Bihan D, Breton E, Lallemand D, Grenier P, Cabanis E, Laval-Jeantet M. MR imaging of intravoxel incoherent motions: application to diffusion and perfusion in neurologic disorders. *Radiology* 1986; 161:401-407.
- Thoeny HC, De Keyser F, Oyen RH, Peeters RR. Diffusion-weighted MR imaging of kidneys in healthy volunteers and patients with parenchymal diseases: initial experience. *Radiology* 2005; 235:911-917.
- Kilickesmez O, Yirik G, Bayramoğlu S, Cimilli T, Aydin S. Non-breath-hold high b-value diffusion-weighted MRI with parallel imaging technique: apparent diffusion coefficient determination in normal abdominal organs. *Diagn Interv Radiol* 2008; 14:83-87.
- Choi YJ, Kim JK, Kim N, Kim KW, Choi EK, Cho KS. Functional MR imaging of prostate cancer. *Radiographics* 2007; 27:63-75.
- Gürses B, Kabakci N, Kovanlikaya A, et al. Diffusion tensor imaging of the normal prostate at 3 Tesla. *Eur Radiol* 2008; 18:716-721.
- Pickles MD, Gibbs P, Sreenivas M, Turnbull LW. Diffusion-weighted imaging of normal and malignant prostate tissue at 3.0T. *J Magn Reson Imaging* 2006; 23:130-134.
- Kim CK, Park BK, Han JJ, Kang TW, Lee HM. Diffusion-weighted imaging of the prostate at 3 T for differentiation of malignant and benign tissue in transition and peripheral zones: preliminary results. *J Comput Assist Tomogr* 2007; 31:449-454.
- Shi H, Ding HY. [Diffusion weighted imaging: its diagnostic and differential value for prostate cancer] [Chinese]. *Zhonghua Nan Ke Xue* 2007; 13:605-609.
- Haider MA, van der Kwast TH, Tanguay J, et al. T2-weighted and diffusion-weighted MRI for localization of prostate cancer. *AJR Am J Roentgenol* 2007; 189:323-328.
- Matsuki M, Inada Y, Tatsugami F, Tanikake M, Narabayashi I, Katsuoka Y. Diffusion-weighted MR imaging for urinary bladder carcinoma: initial results. *Eur Radiol* 2007; 17:201-204.

15. El-Assmy A, Abou-El-Ghar ME, Refaie HF, El-Diasty T. Diffusion-weighted MR imaging in diagnosis of superficial and invasive urinary bladder carcinoma: a preliminary prospective study. *Scientific World Journal* 2008; 8:364–370.
16. Ren J, Huan Y, Wang H, et al. Diffusion-weighted imaging in normal prostate and differential diagnosis of prostate diseases. *Abdom Imaging* 2008 Jan 25. [Epub ahead of print]
17. Carbone SF, Gaggioli E, Ricci V, Mazzei F, Mazzei MA, Volterrani L. Diffusion-weighted magnetic resonance imaging in the evaluation of renal function: a preliminary study. *Radiol Med (Torino)* 2007; 112:1201–1210.
18. Tamada T, Sone T, Toshimitsu S, et al. Age-related and zonal anatomical changes of apparent diffusion coefficient values in normal human prostatic tissues. *J Magn Reson Imaging* 2008; 27:552–556.
19. Miao H, Fukatsu H, Ishigaki T. Prostate cancer detection with 3-T MRI: comparison of diffusion-weighted and T2-weighted imaging. *Eur J Radiol* 2007; 61:297–302.
20. White S, Hricak H, Forstner R, et al. Prostate cancer: effect of postbiopsy hemorrhage on interpretation of MR images. *Radiology* 1995; 195:385–390.
21. Tamada T, Sone T, Jo Y, et al. Prostate cancer: relationships between postbiopsy hemorrhage and tumor detectability at MR diagnosis. *Radiology* 2008; 248:531–539.
22. Koh DM, Scurr E, Collins DJ, et al. Colorectal hepatic metastases: quantitative measurements using single-shot echo-planar diffusion-weighted MR imaging. *Eur Radiol* 2006; 16:1898–1905.